Research Article | Vol. 26, No. 3 | 5 Feb 2018 | OPTICS EXPRESS 2528
Optics EXPRESS

On-chip platform for a phased array with minimal beam divergence and wide field-of-view

MOSHE ZADKA,[1] YOU-CHIA CHANG,[1] ASEEMA MOHANTY,[1,2] CHRISTOPHER T. PHARE,[1,2] SAMANTHA P. ROBERTS,[1] AND MICHAL LIPSON[1,*]

[1] *Department of Electrical Engineering, Columbia University, New York, NY 10027, USA*
[2] *School of Electrical and Computer Engineering, Cornell University, Ithaca, NY 14853, USA*
[*] *ml3745@columbia.edu*

Abstract: Current silicon photonics phased arrays based on waveguide gratings enable beam steering with no moving parts. However, they suffer from a trade-off between beam divergence and field of view. Here, we show a platform based on silicon-nitride/silicon that achieves simultaneously minimal beam divergence and maximum field of view while maintaining performance that is robust to fabrication variations. In addition, in order to maximize the emission from the entire length of the grating, we design the grating's strength by varying its duty cycle (apodization) to emit uniformly. We fabricate a millimeter long grating emitter with diffraction-limited beam divergence of 0.089°.

© 2018 Optical Society of America under the terms of the OSA Open Access Publishing Agreement

OCIS codes: (050.2770) Gratings; (280.3640) Lidar; (190.4390) Nonlinear optics, integrated optics; (250.5300) Photonic integrated circuits.

References and links

1. J. K. Doylend, M. J. R. Heck, J. T. Bovington, J. D. Peters, L. A. Coldren, and J. E. Bowers, "Two-dimensional free-space beam steering with an optical phased array on silicon-on-insulator," Opt. Express **19**, 21595–21604 (2011).
2. D. N. Hutchison, J. Sun, J. K. Doylend, R. Kumar, J. Heck, W. Kim, C. T. Phare, A. Feshali, and H. Rong, "High-resolution aliasing-free optical beam steering," Optica **3**, 887–890 (2016).
3. C. V. Poulton, M. J. Byrd, M. Raval, Z. Su, N. Li, E. Timurdogan, D. Coolbaugh, D. Vermeulen, and M. R. Watts, "Large-scale silicon nitride nanophotonic phased arrays at infrared and visible wavelengths," Opt. Lett. **42**, 21–24 (2017).
4. H. Abediasl and H. Hashemi, "Monolithic optical phased-array transceiver in a standard SOI CMOS process," Opt. Express **23**, 6509–6519 (2015).
5. D. Kwong, A. Hosseini, J. Covey, Y. Zhang, X. Xu, H. Subbaraman, and R. T. Chen, "On-chip silicon optical phased array for two-dimensional beam steering," Opt. Lett. **39**, 941–944 (2014).
6. K. V. Acoleyen, W. Bogaerts, and R. Baets, "Two-Dimensional Dispersive Off-Chip Beam Scanner Fabricated on Silicon-On-Insulator," IEEE Photonics Technol. Lett. **23**, 1270–1272 (2011).
7. M. Raval, C. V. Poulton, and M. R. Watts, "Unidirectional waveguide grating antennas with uniform emission for optical phased arrays," Opt. Lett. **42**, 2563–2566 (2017).
8. D. Taillaert, P. Bienstman, and R. Baets, "Compact efficient broadband grating coupler for silicon-on-insulator waveguides," Opt. Lett. **29**, 2749 (2004).
9. A. Mekis, S. Gloeckner, G. Masini, A. Narasimha, T. Pinguet, S. Sahni, and P. D. Dobbelaere, "A Grating-Coupler-Enabled CMOS Photonics Platform," IEEE J. Sel. Top. Quantum Electron. **17**, 597–608 (2011).
10. G. Roelkens, D. V. Thourhout, and R. Baets, "High efficiency Silicon-on-Insulator grating coupler based on a poly-Silicon overlay," Opt. Express **14**, 11622–11630 (2006).
11. J. Doylend, M. R. Heck, J. Bovington, J. Peters, L. Coldren, and J. Bowers, "Free-space Beam Steering in Two Dimensions Using a Silicon Optical Phased Array," in "Optical Fiber Communication Conference," (Optical Society of America, 2012), p. OM2J.1.
12. C. V. Poulton, A. Yaacobi, D. B. Cole, M. J. Byrd, M. Raval, D. Vermeulen, and M. R. Watts, "Coherent solid-state LIDAR with silicon photonic optical phased arrays," Opt. Lett. **42**, 4091–4094 (2017).
13. K. Shang, C. Qin, Y. Zhang, G. Liu, X. Xiao, S. Feng, and S. J. B. Yoo, "Uniform emission, constant wavevector silicon grating surface emitter for beam steering with ultra-sharp instantaneous field-of-view," Opt. Express **25**, 19655–19661 (2017).
14. X. Chen, C. Li, C. K. Y. Fung, S. M. G. Lo, and H. K. Tsang, "Apodized Waveguide Grating Couplers for Efficient Coupling to Optical Fibers," IEEE Photonics Technol. Lett. **22**, 1156–1158 (2010).

#309928 https://doi.org/10.1364/OE.26.002528
Journal © 2018 Received 25 Oct 2017; revised 11 Jan 2018; accepted 16 Jan 2018; published 24 Jan 2018

Optics EXPRESS

15. R. Waldhäusl, B. Schnabel, P. Dannberg, E.-B. Kley, A. Bräuer, and W. Karthe, "Efficient Coupling into Polymer Waveguides by Gratings," Appl. Opt. **36**, 9383 (1997).

Current silicon photonics phased arrays based on waveguide gratings enable beam steering with no moving parts [1–7], however they suffer from a trade-off between beam divergence (critical for high resolution and long range) and field of view (critical for large steering angle). The beam divergence is determined by the grating's length, which is proportional to the degree of light confinement in the waveguide. For example, in a highly confining platform such as silicon/silicon-dioxide the fully etched grating's length is typically only a few μm [8–10], and even partial etch [11] also results in strong gratings with limited length due to high degree of light confinement. In contrast, in a platform with low degree of light confinement such as silicon-nitride/silicon-dioxide, the grating's length can be as long as 4 mm [3, 7]. The field of view (see ψ in Fig. 1(a)) is determined by the minimal spacing between adjacent waveguides required to avoid crosstalk, which is inversely proportional to the degree of light confinement. For example, in a silicon/silicon-dioxide platform the field of view is expected to be ±50° [3], while for silicon-nitride/silicon-dioxide it is expected to be ±25° [3] due to the large separation required between gratings. We include the coupling lengths of silicon and silicon-nitride based platforms in Fig. 5 in the appendix, showing that for a specific waveguide gap, cross-talk for silicon based platform is smaller than the silicon nitride one. Thus, using silicon as our waveguide enable narrower spacing between waveguides leading to large field of view.

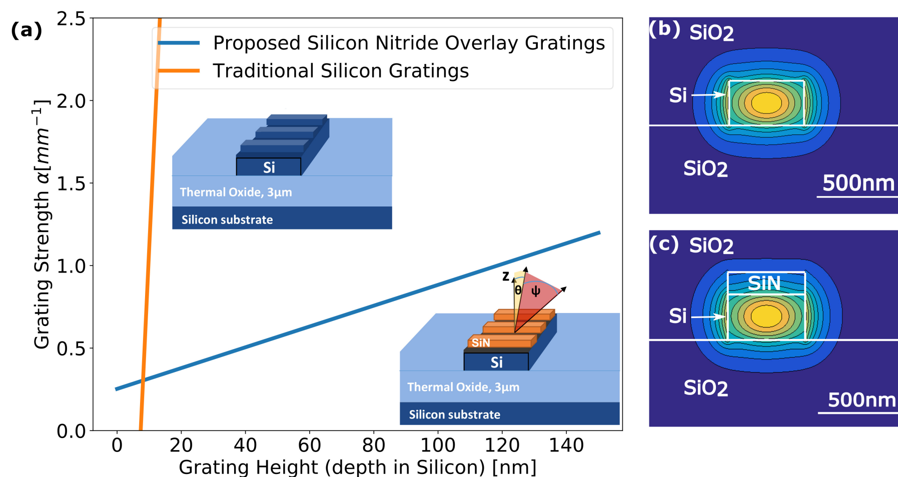

Fig. 1. Simulation of grating's sensitivity to process variations. (a) Strength of grating formed by etching in to a 250 nm x 450 nm silicon waveguide (orange) and by etching a 120 nm silicon nitride overlay on the same silicon waveguide (blue). The period of both gratings is 650 nm. (b) Cross section and spatial mode distribution for the silicon waveguide and (c) for the same waveguide with a silicon nitride overlay and the thin Al_2O_3 between the silicon nitride and silicon. One can see that since the silicon waveguide tightly confines the light, the silicon-nitride overlay only slightly perturb the mode.

Previous attempts to overcome the trade-off between beam divergence and field of view led to performance that is affected by fabrication variations. Hutchison et al. [2] used silicon/silicon-dioxide and was able to fabricate long gratings by reducing the grating's strength using shallow etching of the silicon. Although theoretically this approach could overcome the aforementioned trade-off, in practice, the fabricated gratings are extremely sensitive to variations. Poulton et

Optics EXPRESS

al. [12] reduced the interaction with the mode by fabricating the grating on the side of the waveguide. These grating are, however, sensitive to variations introduced by fabrication. Shang et al. [13] recently demonstrated silicon waveguides with an overlay of silicon-nitride, however these gratings were also shown to be highly sensitive to variations. Figure 1(a), shows the grating's strength sensitivity to etch depth in silicon platform and to nitride thickness for silicon nitride platform. A variation of just 1 nm in the etch depth of silicon/silicon-dioxide grating will increase the grating's strength by more than 11 percent. Controlling the etch depth to that level introduce significant complexity, requiring a challenging fabrication process. In order to find the grating's strength sensitivity in Fig. 1(a), we simulate the grating structure in 2D FDTD and fitted the light emission profile to the conventional exponential decay along the grating (z-axis) that follows:

$$P(z) = P_0 \exp(-2\alpha z) \tag{1}$$

where P_0 is the initial power and α is the grating's coupling strength. Using Eq. (1), we extract the grating's strength for a few representative depths and fit to a line in the region of interest.

We show a hybrid silicon/silicon-nitride grating platform that overcomes the traditional trade-off of phased arrays. This platform enables design tunability of the grating's strength to achieves simultaneously minimal beam divergence in θ axis and maximum field of view in ψ axis. The silicon-nitride overlay perturbs the mode weakly while maintaining high degree of light confinement in the silicon waveguide (Fig. 1(b) and Fig. 1(c)). As the mode distribution is barely disturbed compared with a traditional platform, the grating's strength is less sensitive to fabrication variations. Hence, the grating's strength depends not only on duty cycle but also on the thickness and width of the silicon nitride on the silicon waveguide. The grating's strength sensitivity, which is the slope of the lines in Fig. 1(a), show that the silicon-based grating's is 70 times more sensitive than the silicon-nitride overlay grating. The moderate slope of the silicon-nitride grating enables a process that is robust to fabrication variations as the grating's strength only weakly depend on the silicon-nitride thickness making the fabrication straightforward.

In order to maximize the grating's length, which is determined by the grating's strength along the waveguide length, we design the grating to emit uniformly by varying its duty cycle (apodization). Chen et al. [14] varied the duty cycle ($\frac{\Delta}{\Lambda}$, as in Fig. 2(a)) to maximize the coupling between a fiber and grating. We approximate the uniform emission profile to a flat-top with a

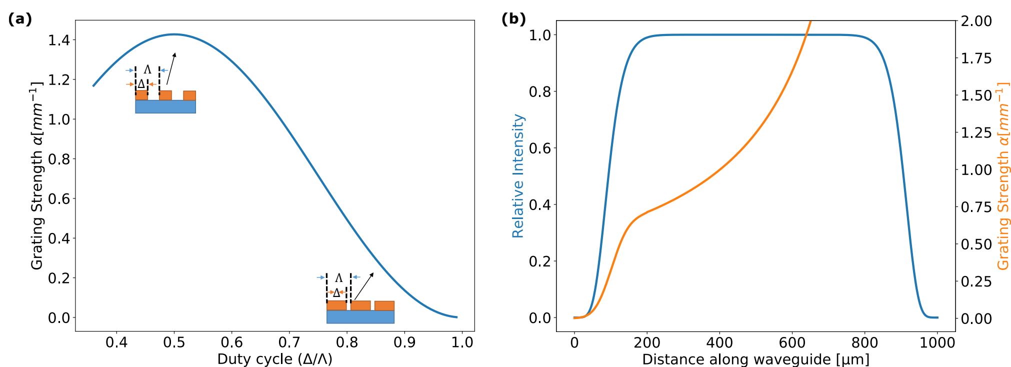

Fig. 2. Grating uniform emission design by apodizing the grating's duty cycle. (a) Grating's strength dependence on duty cycle extracted from 3D FDTD simulations. (b) The desired super-Gaussian emission profile (blue) and its corresponding grating's strength (orange).

Gaussian fall-off also known as super-Gaussian: $SG(z) = A \exp\left[-2\left(\frac{(z-z_0)^2}{w_0^2}\right)\right]$ where $n = 7$ is

Optics EXPRESS

the order, A is the amplitude, z_0 is the center of distribution and $w_0 = 0.5$ mm is the beam waist. Figure 2(b) shows the target emission profile (blue) and the corresponding grating's strength given by [15]:

$$2\alpha(z) = \frac{SG^2(z)}{1 - \int_{z_0}^{z} SG^2(z)dz} \tag{2}$$

Since the emission is proportional to the grating's strength and the amount of light in the waveguide, for uniform output, the grating's strength is low at the input of the waveguide and gradually increases as less light is left in the waveguide. To realize the strength distribution of Fig. 2(a), we vary the grating's duty cycle along the waveguide. Figure 2(a) shows the grating's strength dependence on duty cycle extracted from a 3D FDTD simulation of 100 μm of grating assuming 120 nm overlay of silicon nitride and 250 nm of silicon. As Fig. 2(b) shows, the low-strength grating at the input of the waveguide requires a large duty cycle, which corresponds to a narrow gap $(\Lambda - \Delta)$ of approximately a few nanometers.

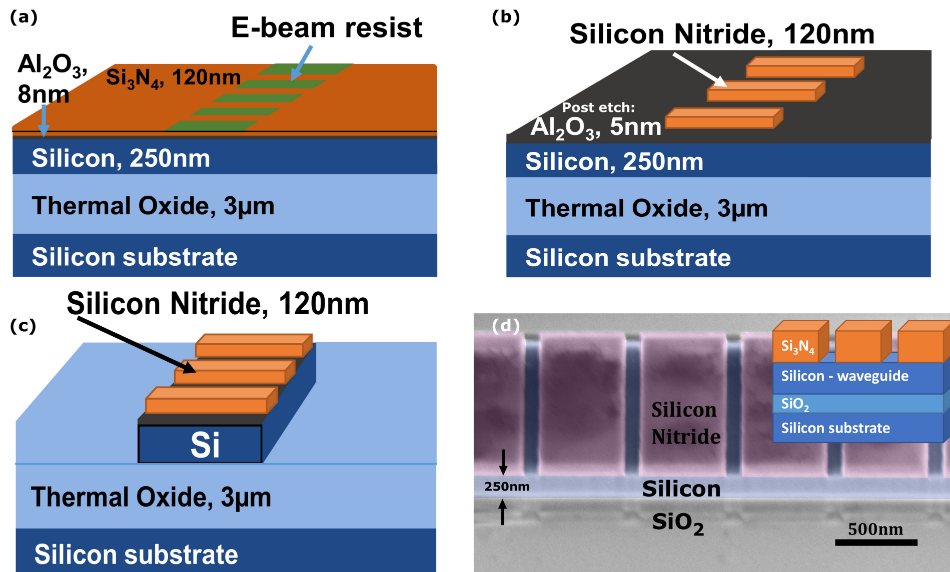

Fig. 3. Platform fabrication steps. (a) Deposition of 8 nm of Al_2O_3 and 120 nm of silicon nitride layers. Defining the grating using E-beam. (b) Etching of silicon-nitride layer and stopping on the Al_2O_3 layer. After etching the silicon nitride, the stop layer thickness is reduced from 8 nm to 5 nm (c) Defining the waveguides using E-beam (450 nm wide), etching, and stopping on the thermal oxide layer. Later, device is cladded with 1 μm of PECVD SiO_2. (d) False-colored tilted Scanning Electron Microscopy picture of the silicon nitride grating overlay after the waveguide etch.

In order to have a process that is both feasible and robust to process variations, we limit the duty cycle to a maximum of 0.85, which for a period of 650 nm corresponds to a gap of about 100 nm. Also, we limit the duty cycle to a minimum of 0.5 to achieve maximum emission (Fig. 2(a)). We fabricate this platform by depositing silicon-nitride as the overlay layer for the gratings and a thin Al_2O_3 layer between the silicon-nitride and silicon to serve as an etch-stop layer when defining the duty cycle. We start with a Silicon-On-Insulator substrate with 250 nm of silicon waveguide layer on top of a 3 μm buried oxide. The 8 nm atomic layer deposited Al_2O_3 layer is thick enough to stop the etch while thin enough to not disturb the mode. We deposit 120 nm of

silicon-nitride using a plasma-enhanced chemical vapor deposition (PECVD) process for the grating (n_{SiN} = 1.99 at 1550 nm), seen in Fig. 3(a). We pattern the grating with electron beam lithography (Elionix) and use CHF_3/O_2 reactive ion etch (RIE) plasma to etch the silicon-nitride and stop on the thin Al_2O_3 layer. Figure 3(b) illustrate the device after we strip off the e-beam resist and clean the chip in piranha acid (3:1 $H_2SO_4 : H_2O_2$). We pattern the waveguides using e-beam lithography (450 nm wide) and etch using C_4HF_8 based RIE, stopping on the thermal oxide layer and strip and clean the sample (Fig. 3(c)). Finally, we deposit a 1 μm cladding layer of SiO_2 using PECVD. Figure 3(d) shows a tilted scanning electron microscope image of the device before the cladding.

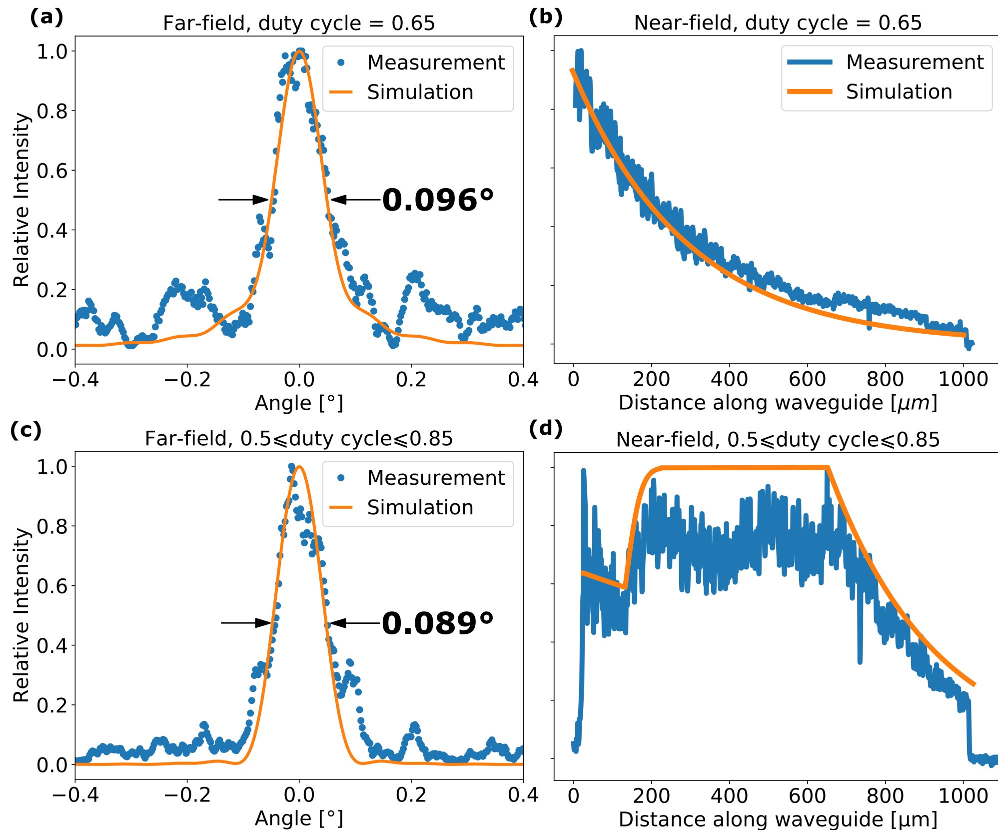

Fig. 4. Near-field and far-field measurements and simulations for silicon-nitride/silicon platform. (a) and (c) Far-field measurement and simulations for 1 mm grating with a constant and apodized duty cycle, respectively. (b) and (d) Near-field grating emission profile of constant and apodized duty cycle, respectively. As expected, although the gratings' lengths are the same, the larger effective aperture of the apodized grating enabled smaller beam divergence.

Using this platform, we demonstrate a millimeter long diffraction-limited emitter with a beam divergence of 0.089°. We measure the beam divergence by placing a lens (f=500 mm) at the focal plane between the chip and an infrared camera (Xenics), obtaining the far-field diffraction pattern. The long focal length lens coupled with the camera's small pixel pitch (20 μm) allows for high-resolution measurement. In order to show the importance of the duty cycle apodization, we measure the beam divergence of both a grating with constant duty cycle and an apodized

one. The measurement show a beam divergence of 0.096° for the constant duty cycle grating and a diffraction limited beam divergence of 0.089° for the apodized grating (Fig. 4(a) and Fig. 4(c), respectively). We find that, as expected, although the gratings' lengths are the same, the larger effective aperture of the apodized grating enabled smaller beam divergence. The small lobes are due to scattering from point defects in the waveguide. In order to measure the emission profile, we image the near-field output using 20X microscope objective, which allow capturing the emission of the 1 mm long gratings in two frames. This reduces the stitching errors while maintaining high resolution.

We have demonstrated a platform that overcomes the traditional limitations of silicon photonics phased arrays. We show that it is possible to have both minimal beam divergence typically obtained only in low index contrast platforms while still maintaining large field of view as obtained in high index-contrast platforms. Our demonstration of beam divergence of 0.089° for a millimeter long waveguide while using a process that is robust to fabrication variations illustrates the usefulness of this platform for potential applications in phased arrays for LiDAR (Light Detection and Ranging), wireless communications, and particle trapping.

Appendix: Comparison of silicon and silicon nitride platforms coupling lengths

In order to highlight the fundamental ability to increase the packing density we calculate the theoretical coupling length corresponding to 100 percent power transfer between two of our waveguides and between two typical silicon nitride waveguides, for different gap lengths. Figure 5 shows that for a given coupling length (i.e. cross-talk level) the required gap between the silicon waveguides is much narrower than one required between the silicon nitride waveguides, thus enabling a more tightly packed array.

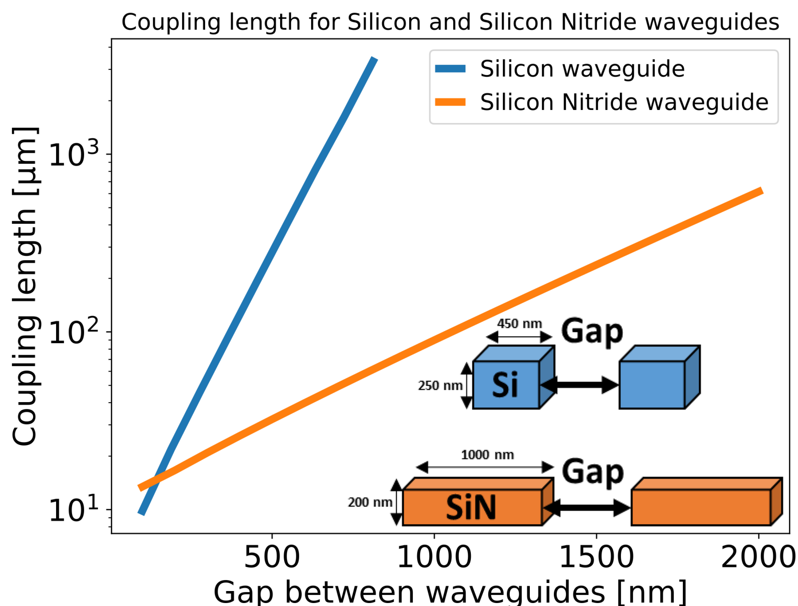

Fig. 5. Coupling length for silicon and silicon nitride waveguides. Due to the strong light confinement in the silicon, the coupling length is longer than in silicon nitride waveguide, thus the silicon waveguides exhibit smaller amount of cross-talk and could be tightly packed.

Funding

Defense Advanced Research Projects Agency (DARPA) (HR0011-16-C-0107).

Optics EXPRESS

Acknowledgments

This work was performed in part at the CUNY Advanced Science Research Center NanoFabrication Facility.

128.59.65.215 {ts '2018-01-24 19:17:40'}